J|A|C|S
ARTICLES

Mesoporous Co_3O_4 and Au/Co_3O_4 Catalysts for Low-Temperature Oxidation of Trace Ethylene

Chun Yan Ma,[†] Zhen Mu,[†] Jin Jun Li,[†] Yong Gang Jin,[‡] Jie Cheng,[†] Gao Qing Lu,[‡] Zheng Ping Hao,*,[†] and Shi Zhang Qiao*,[‡]

State Key Laboratory of Environmental Chemistry and Ecotoxicology, Research Center for Eco-Environmental Sciences, Chinese Academy of Sciences, Beijing 100085, P. R. China, and ARC Centre of Excellence for Functional Nanomaterials, Australian Institute for Bioengineering and Nanotechnology, The University of Queensland, QLD 4072, Australia

Received August 2, 2009; E-mail: zpinghao@rcees.ac.cn; s.qiao@uq.edu.au

Abstract: Low-temperature catalysts of mesoporous Co_3O_4 and Au/Co_3O_4 with high catalytic activities for the trace ethylene oxidation at 0 °C are reported in this paper. The catalysts were prepared by using the nanocasting method, and the mesostructure was replicated from three-dimensional (3D) cubic KIT-6 silicas. High resolution transmission electron microscopy (HRTEM) studies revealed that {110} facets were the exposed active surfaces in the mesoporous Co_3O_4, whereas the Co_3O_4 nanosheets prepared by the precipitation method exhibited the most exposed {112} facets. We found that the mesoporous Co_3O_4 was significantly more active for ethylene oxidation than the Co_3O_4 nanosheets. The results indicated that the crystal facet {110} of Co_3O_4 played an essential role in determining its catalytic oxidation performance. The synthesized Au/Co_3O_4 materials, in which the gold nanoparticles were assembled into the pore walls of the Co_3O_4 mesoporous support, exhibited stable, highly dispersed, and exposed gold sites. Gold nanoparticles present on Co_3O_4 readily produced surface-active oxygen species and promoted ethylene oxidation to achieve a 76% conversion at 0 °C, which is the highest conversion reported yet.

1. Introduction

Chemists and material scientists are driven to improve the performance of materials for technological applications. Materials' functions depend on their compositions, crystal structures, and morphologies. The properties of materials with the same composition but different structure or morphologies can vary substantially.[1−4] Scientists directed increasingly more effort on nanostructural organization to design functional materials.[5] The fundamental understanding has showed that structure and morphology control of base transition-metal oxides allows preferential exposure of catalytically active sites.[6]

Co_3O_4 has been reported to be an effective catalyst in the oxidation reaction and has also been used as a support for noble metals. Co_3O_4 is a versatile oxide that is involved in many advanced physical applications (magnetic properties) and in various heterogeneous catalysis processes, for example, NO_x reduction,[7] CO oxidation (with[8,9] or without gold promoter[10]),

and vapor-phase oxidation of organic molecules.[11] Co_3O_4 with different morphologies or structures such as nanospheres, nanocubes, nanorods, and mesoporous structures has been reported.[9,12−16] The properties of the as-synthesized Co_3O_4 materials strongly depend on their morphologies, crystal sizes, and exposed crystal facets.[6,9,12,17−19] However, Co_3O_4 catalysts are usually composed of assorted polycrystals with different exposed crystal facets, possessing several kinds of active sites, which exhibit different reactivities and usually with lower catalytic activities.[9,12] Recently, Hu et al.[12] reported that the unusually high index {112} crystal facets of Co_3O_4 nanosheets were more reactive than the {011} facets of Co_3O_4 nanobelts

[†] Chinese Academy of Sciences.
[‡] The University of Queensland.
(1) Iijima, S. *Nature* **1991**, *354*, 56–58.
(2) Pai, R. A.; Humayun, R.; Schulberg, M. T.; Sengupta, A.; Sun, J. N.; Watkins, J. J. *Science* **2004**, *303*, 507–510.
(3) Yang, H. G.; Sun, C. H.; Qiao, S. Z.; Zou, J.; Liu, G.; Smith, S. C.; Cheng, H. M.; Lu, G. Q. *Nature* **2008**, *453*, 639–641.
(4) Yang, H. G.; Liu, G.; Qiao, S. Z.; Sun, C. H.; Jin, Y. G.; Smith, S. C.; Zou, J.; Cheng, H. M.; Lu, G. Q. (Max) *J. Am. Chem. Soc.* **2009**, *131*, 4078–4083.
(5) Cölfen, H.; Mann, S. *Angew. Chem., Int. Ed.* **2003**, *42*, 2350–2365.
(6) Cao, A.-M.; Hu, J.-S.; Liang, H.-P.; Song, W.-G.; Wan, L.-J.; He, X.-L.; Gao, X.-G.; Xia, S.-H. *J. Phys. Chem. B* **2006**, *110*, 15858–15863.
(7) Wichterlová, B. *Top. Catal.* **2004**, *28*, 131–140.

(8) Xu, X. Y.; Li, J. J.; Hao, Z. P.; Zhao, W.; Hu, C. *Mater. Res. Bull.* **2006**, *41*, 406–413.
(9) Xie, X.; Li, Y.; Liu, Z.-Q.; Haruta, M.; Shen, W. *Nature* **2009**, *458*, 746–749.
(10) Wang, C. B.; Tang, C. W.; Gau, S. J.; Chien, S. H. *Catal. Lett.* **2005**, *101*, 59–63.
(11) Vetrivel, S.; Pandurangan, A. *J. Mol. Catal. A: Chem.* **2005**, *22*, 269–278.
(12) Hu, L.; Peng, Q.; Li, Y. *J. Am. Chem. Soc.* **2008**, *130*, 16136–16137.
(13) He, T.; Chen, D. R.; Jiao, X. L.; Xu, Y. Y.; Gu, Y. X. *Langmuir* **2004**, *20*, 8404–8408.
(14) Wang, Y. Q.; Yang, C. M.; Schmidt, W.; Spliethoff, B.; Bill, E.; Schüth, F. *Adv. Mater.* **2005**, *17*, 53–56.
(15) Lakshmi, B. B.; Patrissi, C. J.; Martin, C. R. *Chem. Mater.* **1997**, *9*, 2544–2550.
(16) Feng, J.; Zeng, H. C. *Chem. Mater.* **2003**, *15*, 2829–2835.
(17) Tian, Z. R. R.; Voigt, J. A.; Liu, J.; McKenzie, B.; McDermott, M. J.; Rodriguez, M. A.; Konishi, H.; Xu, H. F. *Nat. Mater.* **2003**, *2*, 821–826.
(18) Hu, J. S.; Ren, L. L.; Guo, Y. G.; Liang, H. P.; Cao, A. M.; Wan, L. J.; Bai, C. L. *Angew. Chem., Int. Ed.* **2005**, *44*, 1269–1273.
(19) Li, W. Y.; Xu, L. N.; Chen, J. *Adv. Funct. Mater.* **2005**, *15*, 851–857.

and {001} facets of Co$_3$O$_4$ nanocubes for methane catalytic combustion. While Xie et al.[9] reported that the Co$_3$O$_4$ nanorods, which predominantly exposed their {110} facets, favoring the presence of active Co^{3+} species at the surface, exhibited a much higher activity for CO oxidation than that of conventional nanoparticles which mainly exposed the {001} and {111} facets, containing only inactive Co^{2+} sites. Therefore, the selective synthesis of nanostructured Co$_3$O$_4$ catalysts with highly reactive crystal facets under nanoscale is a key to exploring different catalytic properties and applications.

Many efforts have been made to obtain porous Co$_3$O$_4$ particles with controlled dimensions via nanocasting, i.e., by crystallizing inside the pores of both aperiodic and periodic silicas (commercial monoliths, MCM, SBA).[10,11,20−25] Basic issues on the nanocasting strategy have been recently reviewed.[26] However, very few published results are available on the reactive crystal planes of Co$_3$O$_4$ materials prepared using the nanocasting method and their correlation with catalytic reaction activity.

Highly dispersed Au nanoparticles supported on metal oxides can show exceptionally high activities for several kinds of reactions including CO oxidation, ozone decomposition, oxidation of hydrogen, and the CO + NO reaction.[27−30] Many studies have focused on the unusual low-temperature activity and the activation mechanism of gold catalysts.[31−34] The efficiency of supported Au nanoparticles for a low-temperature reaction depends on a variety of factors including, for example, the sizes of Au particles, the properties of supports, and their preparation procedures and pretreatment conditions. Although the support has activity in some reactions such as CO oxidation, the highly dispersed Au nanoparticles appear to be responsible for the high activity of supported catalysts.[35,36]

Ethylene, a low molecular weight volatile organic compound (VOC) that possesses both C−C σ and C−C π bonds, is harmful, causing anesthetic illness and enhancing photochemical pollution. It is thus worthwhile to remove trace ethylene from some environments. For example, in fruit stores (such as refrigerated warehouses), ethylene released from fruits can accelerate aging and spoiling of produce.[37,38] In order to maintain freshness, the elimination of trace ethylene at low temperature (0 °C) is required. Although the oxidation of ethylene is a thermodynamically favored process, ethylene is thermally stable and usually oxidized in the presence of catalysts. Until now, only limited solid thermal catalysts have been reported, but their catalytic activities are not sufficient and the operating temperatures are higher than 100 °C.[38] To the best of our knowledge, there has not been any report on ethylene oxidation over solid thermal catalysts at 0 °C. It is very difficult to activate and break the C−C σ bond of ethylene (unlike HCHO and CO) at a low reaction temperature of 0 °C; thus, more powerful catalytic materials are desirable.

Our recent work revealed that the Co$_3$O$_4$ catalyst prepared by a precipitation method had no catalytic activity of trace ethylene oxidation at 20 °C, and the Au/Co$_3$O$_4$ catalyst, with 2% gold loading prepared by a deposition−precipitation method, converted 7.4% of trace ethylene at 20 °C.[30] Thus, this catalyst is not suitable in the elimination of trace ethylene because of its insufficient activity at low temperature, as it cannot efficiently activate ethylene and break its C−C σ bond and produce carbon dioxide. Furthermore, the catalytic activation mechanism of Co$_3$O$_4$ and Au/Co$_3$O$_4$ catalysts in ethylene oxidation was still not clearly discussed.

Herein, we report the development of low-temperature catalysts of mesoporous Co$_3$O$_4$ and Au/Co$_3$O$_4$ and their excellent catalytic performance on the oxidation elimination of trace ethylene at low temperatures. We found more enhanced catalytic activity for ethylene oxidation over mesoporous Co$_3$O$_4$ prepared by the nanocasting method compared with Co$_3$O$_4$ nanosheets prepared by the precipitation method. The roles of the active crystal facets {110} of Co$_3$O$_4$ catalysts on ethylene oxidation are discussed in this paper. Furthermore, we found that the mesoporous Au/Co$_3$O$_4$ catalyst exhibited well-distributed Au nanoparticles on the porous Co$_3$O$_4$ matrix, which provided a greater number of active gold sites and led to high catalytic activity for ethylene oxidation (76% conversion) at 0 °C. This is the highest reported conversion of ethylene oxidation at a low temperature. The study of the catalytic activation mechanism presented here is critically important to enhancing low-temperature catalytic activities in various oxidation reactions.
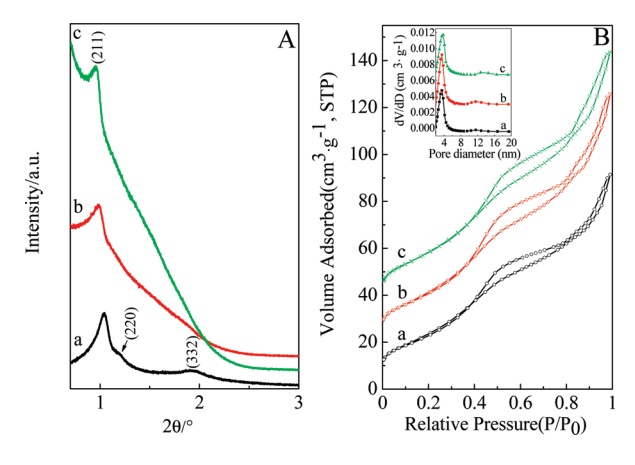
2. Results and Discussion

2.1. Synthesis and Characterization of Co$_3$O$_4$ and Au/Co$_3$O$_4$ Materials. The synthesis of mesoporous Co$_3$O$_4$ material involves three substeps: (1) the impregnation and thermal decomposition of a cobalt precursor in the pore of three-dimensional (3D) cubic KIT-6 silica with an *ia3d* mesostructure (hard template, see Figure S1−S3 in the Supporting Information for relative characterizations); (2) the repeated impregnation and decomposition steps; (3) the removal of the hard template by NaOH solution etching. The obtained Co$_3$O$_4$ grows along the direction of the KIT-6 channels and replicates the 3D mesoporous structure of KIT-6. The preparation of the mesoporous Au/Co$_3$O$_4$ sample follows the same steps as in the synthesis of mesoporous Co$_3$O$_4$ above but also involves impregnation of cobalt and gold precursors together. It is widely recognized that active phase dispersion is greatly influenced by the affinity of

(20) Martinez, A.; Lopez, C.; Marquez, F.; Dias, J. *J. Catal.* **2003**, *220*, 486−499.
(21) Ohtsuka, Y.; Takahashi, Y.; Noguchi, M.; Arai, T.; Tarasaki, S.; Tsubouchi, N.; Wang, Y. *Catal. Today* **2004**, *89*, 419−429.
(22) Khodakov, A. Y.; Griboval-Constant, A.; Bechara, R.; Zholobenko, V. L. *J. Catal.* **2002**, *206*, 230−241.
(23) Tian, B. Z.; Liu, X.; Solovyov, L.; Liu, Z.; Zang, H.; Zhang, Z.; Xie, S.; Zhang, F.; Tu, B.; Yu, C.; Terasaki, O.; Zhao, D. *J. Am. Chem. Soc.* **2004**, *126*, 865−875.
(24) Crowley, T. A.; Ziegler, K. J.; Lyons, D. M.; Erst, D.; Olin, M.; Morin, M. A.; Holmes, J. D. *Chem. Mater.* **2003**, *15*, 3518−3522.
(25) Smatt, J. H.; Spliethoff, B.; Rosenholm, J. B.; Linden, M. *Chem. Commun.* **2004**, *2188*, 2189.
(26) Liu, A. H.; Schüth, F. *Adv. Mater.* **2006**, *18*, 1793−1805.
(27) Haruta, M.; Tsbota, S.; Kobayashi, T.; Kageyama, H.; Genet, M. J.; Delmon, B. *J. Catal.* **1993**, *144*, 175−192.
(28) Hao, Z. P.; An, L. D.; Zhou, J. L.; Wang, H. L. *React. Kinet. Catal. Lett.* **1996**, *59*, 295−300.
(29) Hao, Z. P.; Cheng, D. Y.; Guo, Y.; Liang, Y. H. *Appl. Catal., B* **2001**, *33*, 217−222.
(30) Li, J. J.; Ma, C. Y.; Xu, X. Y.; Yu, J. J.; Hao, Z. P.; Qiao, S. Z. *Environ. Sci. Technol.* **2008**, *42*, 8947−8951.
(31) Tsai, H.-Y.; Lin, Y.-D.; Fu, W.-T.; Lin, S. D. *Gold Bull.* **2007**, *43*, 184−191.
(32) Daté, M.; Okumura, M.; Tsubota, S.; Haruta, M. *Angew. Chem., Int. Ed.* **2004**, *43*, 2129−2132.
(33) Chen, Z.; Gao, Q. *Appl. Catal., B* **2008**, *84*, 790−796.
(34) Dobrosz-Gómez, I.; Kocemba, I.; Rynkowski, J. M. *Appl. Catal., B* **2008**, *83*, 240−255.
(35) Dobrosz-Gómez, I.; Kocemba, I.; Rynkowski, J. M. *Appl. Catal., B* **2008**, *83*, 240−255.
(36) Chen, Z.; Gao, Q. *Appl. Catal., B* **2008**, *84*, 790−796.
(37) Park, D. R.; Ahn, B.-J.; Park, H.-S.; Yamashita, H.; Anpo, M. *Korean J. Chem. Eng.* **2001**, *18*, 930−934.
(38) Ahn, H. G.; Choi, B. M.; Lee, D. J. *J. Nanosci. Nanotechnol.* **2006**, *6*, 3599−3603.
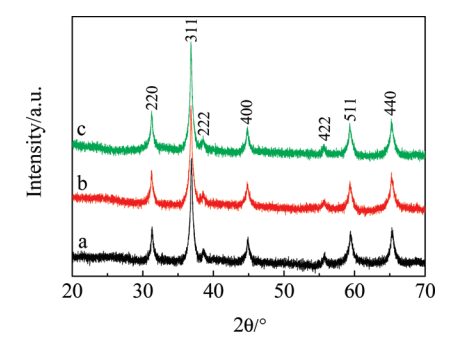
Figure 1. (A) Low-angle XRD patterns and (B) N_2 adsorption/desorption isotherms (inset: pore size distribution calculated from desorption branch) of the mesoporous Co_3O_4 and Au/Co_3O_4 materials with different gold loadings: (a) Co_3O_4, (b) 1.0% Au/Co_3O_4, (c) 2.5% Au/Co_3O_4. The isotherm curves b and c in panel B are shifted by 15 and 30 $cm^3 \cdot g^{-1}$, STP, respectively, for clarity.

the precursor to the support, and that this strong affinity facilitates good dispersion.[39] When mesoporous Au/Co_3O_4 is synthesized, hydrolysis and aging of the gold chloride ($HAuCl_4$) solution at different pH conditions may vary the concentration of various gold species $[Au(OH)_nCl_{4-n}]^-$ ($n = 1$–3). The strongly adsorbing species $Au(OH)_3Cl^-$ can be obtained at pH 7. Therefore, in this work the well-dispersed gold nanoparticles attached to the Co_3O_4 support were synthesized at pH 7. In the impregnation process, the solution mixture containing $Au(OH)_3Cl^-$ and Co^{2+} precursor was introduced into the pores of KIT-6. After the samples were calcined and the hard template KIT-6 was removed, ordered mesoporous Co_3O_4 was obtained as a faithful replica of the template KIT-6 and the gold nanoparticles were strongly adsorbed/embedded on the mesoporous Co_3O_4 base.

The low-angle X-ray diffraction (XRD) patterns of Co_3O_4 and Au/Co_3O_4 samples, with different Au contents, synthesized using KIT-6 as templates are shown in Figure 1A. Figure 1A(a) shows well-resolved diffraction peaks (211) and (332), and the shoulder peak (220), which are characteristic of a cubic *ia3d* mesostructure, indicating a high degree of ordering of the mesoporous Co_3O_4 material. Mesoporous Co_3O_4 material is well-resolved in comparison to the characteristic diffraction peaks from its template KIT-6 (see Figure S1 in Supporting Information), indicating that the mesostructure of the Co_3O_4 samples is a negative replica of KIT-6. A decrease of the structural ordering with an increase of the gold content can also be found for various Au/Co_3O_4 catalysts. It shows that the adjustment of the pH value and the production of $[Au(OH)_nCl_{4-n}]^-$ may interrupt the impregnation and decomposition of a cobalt precursor in the silica pore. Large angle XRD patterns of mesoporous Co_3O_4 and Au/Co_3O_4 materials exhibit peaks at 31.3°, 36.9°, 38.2°, 44.5°, 55.6°, 59.4°, and 65.3° (2θ),[40] indicating that the cobalt precursor is turned completely into crystalline cobalt oxide (Figure 2). The diffraction peak at 38.2° corresponds to the Co_3O_4 (222) plane. Because the Au^0 (111) diffraction peak overlaps with the Co_3O_4 (222) diffraction peaks, it is difficult and not meaningful to calculate the gold particle size using the Scherrer equation.

Figure 2. Large-angle XRD patterns of the mesoporous Co_3O_4 and Au/Co_3O_4 materials. (a) Co_3O_4, (b) 1.0% Au/Co_3O_4, (c) 2.5% Au/Co_3O_4.

Table 1. Ethylene Oxidation Activities and Physical Properties of Co_3O_4 and Au/Co_3O_4 Catalysts[a]

catalysts	C_2H_4 conversion (%)	S_{BET}[b] (m²/g)	V_p[c] (cm³/g)	D_p[d] (nm)
Co_3O_4 (3D)	30 (0 °C)	84	0.14	3.6/11.7
1.0% Au/Co_3O_4 (3D)	50 (0 °C)	94	0.17	3.4/11.4
2.5% Au/Co_3O_4 (3D)	76 (0 °C)	100	0.18	3.4/11.5
Co_3O_4[e] (P)	0 (20 °C)	–	–	–
2% Au/Co_3O_4[e] (DP)	7.4 (20 °C)	–	–	–

[a] Initial concentration of ethylene is 50 ppm. [b] BET specific surface areas determined from the linear part of the BET equation ($P/P_0 = 0.05$–0.25). [c] Total pore volumes obtained at $P/P_0 = 0.99$. [d] Pore size determined from the desorption branch using the BJH method. [e] Reproduced with permission from ref 7. P: precipitation method, DP: deposition–precipitation method.

The N_2 sorption results (Figure 1B) show that all of the mesoporous Co_3O_4 and Au/Co_3O_4 materials exhibit type IV isotherms (IUPAC classification), indicating the presence of mesopores.[41,42] However, the capillary condensation step of mesoporous Au/Co_3O_4 is not very pronounced, indicating the relatively small sizes of ordered domains.[43] Nitrogen physisorption data are in good agreement with the low-angle XRD results. The Barrett–Joyner–Halenda (BJH) pore size distributions of the mesoporous Co_3O_4 and Au/Co_3O_4 materials are shown in the inset of Figure 1B. The Co_3O_4 and Au/Co_3O_4 materials have two primary mesopore diameters of 3.4 and 11.5 nm, respectively. A broad peak of pore size distribution at 11.5 nm is probably attributed to interspace of the samples. Table 1 shows structure parameters of the Co_3O_4 and Au/Co_3O_4 catalysts. The mesopore diameters of Au/Co_3O_4 samples do not decrease remarkably with the increase of gold loading, indicating that most Au particles are studded on the surface or embedded in the pore wall. The Brunauer–Emmett–Teller (BET) surface areas (Table 1) of the mesoporous Co_3O_4 and Au/Co_3O_4 materials synthesized by the nanocasting method are much larger than those of the Co_3O_4 samples prepared by the precipitation method (about 15 $m^2 \cdot g^{-1}$).[30]

High angular annular dark-field scanning transmission electron microscopy (HAADF-STEM) images of the mesoporous 2.5% Au/Co_3O_4 materials are shown in Figure 3. The support Co_3O_4 has $Ia3d$ symmetry and ordered mesostructures. The gold nanoparticles (smaller than 5 nm), imaged as white luminous dots, are presented as pseudospherical particles and incorporated in the Co_3O_4 matrix. Such a mesoporous structure can thus

(39) Lee, S.-J.; Gavriilidis, A. *J. Catal.* **2002**, *206*, 305–313.
(40) Li, J. J.; Xu, X. Y.; Hao, Z. P.; Zhao, W. *J. Porous Mater.* **2008**, *15*, 163–169.
(41) Sing, K. S. W.; Evrett, D. H.; Haul, R. A. W.; Moscou, L.; Pierotti, R. A.; Rouquérol, J.; Siemieniewska, T. *Pure Appl. Chem.* **1985**, *57*, 603–619.
(42) Kruk, M.; Jaroniec, M. *Chem. Mater.* **2001**, *13*, 3169–3183.
(43) Rumplecker, A.; Kleitz, F.; Salabas, E.-L.; Schüth, F. *Chem. Mater.* **2007**, *19*, 485–496.
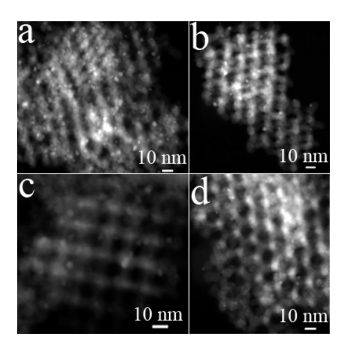
Figure 3. HAADF-STEM images of the mesoporous 2.5% Au/Co₃O₄ materials observed along different directions.
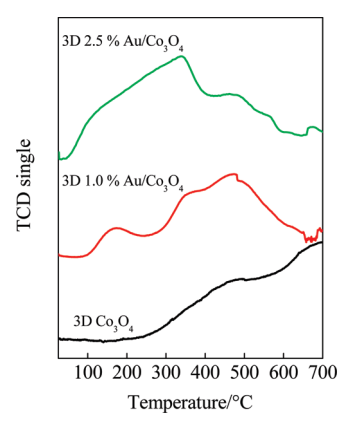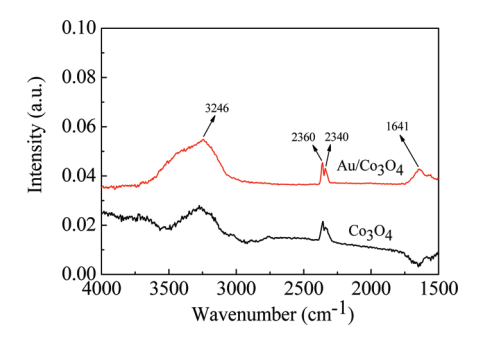

Figure 4. O_2–TPD profiles of mesoporous Co_3O_4 and Au/Co_3O_4 with different gold loadings.

effectively prevent gold nanoparticles from both aggregation and leaching because of the confinement of the channels. We can also note that the mesoporous channels are not blocked by the gold nanoparticles, thus greatly facilitating the transport of both reactant and product. For mesoporous Au/Co_3O_4 materials, gold particles enter pores, embed into pore walls, and drill through the Co_3O_4 walls, which may offer more active sites for the catalytic reaction.

Figure 4 shows the O_2–temperature-programmed desorption (O_2–TPD) profiles of the fresh catalysts. The peak below 300 °C is ascribed to the desorption of surface-active oxygen species such as O_2^- and O^-, and the desorption peak above 350 °C is attributable to the desorption of lattice oxygen in Co_3O_4.[44] Generally speaking, the larger the corresponding desorption peak area of surface-active oxygen species at the low-temperature range, the higher the catalytic ability for oxidation reaction.[29] A broad and strong desorption peak from 50 to 300 °C for the 2.5% Au/Co_3O_4 sample is evident. In contrast, a small desorption peak can be detected in Co_3O_4 in a similar temperature range. Both surface-active oxygen species and lattice oxygen desorption peaks can also be observed in the O_2–TPD profiles of the 1.0% Au/Co_3O_4 samples. It is clear that the surface-active oxygen species of the Au/Co_3O_4 catalysts increase with increasing gold content.

Figure 5 shows the diffuse reflectance infrared Fourier transform (DRIFT) spectra of surface species on mesoporous Co_3O_4 and Au/Co_3O_4 samples at 25 °C in a flow of 50 ppm C_2H_4/22% O_2/He. Several IR peaks are observed in the range of 1500 to 4000 cm⁻¹. The bands appearing at 2340 and 2360

Figure 5. DRIFT spectra of ethylene oxidation on mesoporous Co_3O_4 and 2.5% Au/Co_3O_4 catalysts.

cm⁻¹ are ascribed to the asymmetric stretch, $\nu_{asym}(OCO)$, of CO_2 molecules adsorbed on the catalysts.[45] The bands observed around 1641 and 3246 cm⁻¹ are attributed to the stretching vibration of carbon–carbon double bonds, $\nu(C=C)$, and the vibration of carbon–hydrogen bonds, $\nu(C-H)$, of C_2H_4 molecules, respectively.[45,46] Compared with Co_3O_4, the intensity of peak at 1641 cm⁻¹ on Au/Co_3O_4 increases, which suggests a relatively strong adsorption of reactant C_2H_4. Apart from C_2H_4 and CO_2, no other ethylene oxides are detected in DRIFT measurements on mesoporous Co_3O_4 and Au/Co_3O_4 catalysts, thus indicating that only the complete oxidation of ethylene to CO_2 occurs.

2.2. Low-Temperature Activity of Ethylene Oxidation. An ethylene concentration of 50 ppm in the initial gas was used to investigate catalyst activity in this study. Table 1 also exhibits an ethylene conversion over Co_3O_4 and Au/Co_3O_4 catalysts. It is evident that the preparation method has a significant influence on catalytic performance. The 2.0% Au/Co_3O_4 catalyst prepared by the deposition–precipitation method was less active at 0 °C and can oxidize only 7.4% ethylene at 20 °C. The Co_3O_4 catalyst (without nanogold loading) prepared by the precipitation method does not have any ethylene oxidation activity even at 20 °C. In contrast, the mesoporous Co_3O_4 catalysts prepared using the nanocasting method drastically enhance the activity of ethylene oxidation, with an ethylene conversion of 30% at 0 °C. In addition, the activity of mesoporous Au/Co_3O_4 catalysts prepared using the nanocasting method is further enhanced when nanogold is introduced. The percentage of ethylene conversion is 50% over mesoporous 1.0% Au/Co_3O_4 catalyst at 0 °C. The mesoporous 2.5% Au/Co_3O_4 catalyst shows much higher activity at 0 °C (76% conversion of ethylene), which is around ten times the activity of the 2.0% Au/Co_3O_4 catalyst at 20 °C prepared by the deposition–precipitation method.
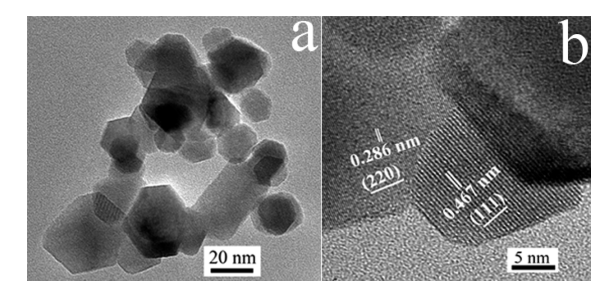
2.3. Correlation between Catalyst Structure and Activity. In this work, the mesoporous Co_3O_4 samples replicate the 3D mesostructure of the KIT-6. Mesoporous Co_3O_4 shows around 30% ethylene conversion to CO_2 at 0 °C. However, the Co_3O_4 nanosheets prepared by the precipitation method have no activity of ethylene oxidation at 20 °C. This indicates that structural control of Co_3O_4 allows the preferential exposure of catalytically active sites. Figures 6 and 7 show HRTEM images of the Co_3O_4 nanosheets prepared by the precipitation method and the mesoporous Co_3O_4 and Au/Co_3O_4 synthesized via nanocasting, respectively. The Co_3O_4 nanosheets are hexagonal in shape with size ca. 20–50 nm. Both a set of {220} planes with a lattice

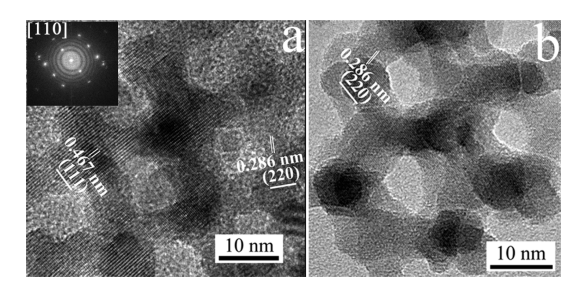(44) Xue, L.; Zhang, C.; He, H.; Teraoka, Y. *Appl. Catal., B* **2007**, *75*, 167–174.

(45) Berná, A.; Kuzume, A.; Herrero, E.; Feliu, J. M. *Surf. Sci.* **2008**, *602*, 84–94.

(46) Chen, X.-M.; Yang, X.-F.; Zhu, A.-M.; Fan, H.-Y.; Wang, X.-K.; Xin, Q.; Zhou, X.-R.; Shi, C. *Catal. Commun.* **2009**, *10*, 428–432.

Figure 6. (a) TEM image and (b) HRTEM image of Co_3O_4 nanosheets prepared by the precipitation method.

Figure 7. HRTEM images of mesoporous Co_3O_4 (a) and Au/Co_3O_4 (b) prepared by the nanocasting method. The insert in panel a is the FFT diffractogram of the corresponding HRTEM image.

space of 0.286 nm and a set of {111} planes with a square crossing lattice space of 0.467 nm were observed for Co_3O_4 nanosheets (Figure 6b). The dominant exposed planes of Co_3O_4 nanosheets are {112}, which are perpendicular to both the first set of (220) planes and the second set of (222) planes.[12] Figure 7 shows HRTEM images of typical mesoporous Co_3O_4 and Au/Co_3O_4. The upper left inset in Figure 7a shows the fast Fourier transform (FFT) diffractogram from the mesoporous Co_3O_4 with [110] direction. Figure 7a shows that the lattice planes of mesoporous Co_3O_4 are both {111} with a lattice space of 0.467 nm and {220} with a lattice space of 0.286 nm. The {111} planes are believed to be inactive crystal planes.[9] Furthermore, {220} planes with a lattice space of 0.286 nm were also observed for mesoporous Au/Co_3O_4 (Figure 7b). For the mesoporous Co_3O_4 and Au/Co_3O_4, the exposed active planes are {110} planes parallel to {220}. The {110} planes are composed mainly of Co^{3+} cations, and the abundant Co^{3+} cations on the {110} planes provide sufficient sites for ethylene and oxygen adsorption and are regarded as the active sites for ethylene oxidation. When the reactants passed through and adsorbed into the pores of mesoporous Co_3O_4, they were activated by the exposed facets. Thus, we can conclude that the {110} planes are the mainly active planes for ethylene oxidation. This is in accord with recently published significant research, in which low-temperature oxidation of CO on Co_3O_4 nanorods was systematically studied.[9]

In the preparation of mesoporous Au/Co_3O_4, the precursor $AuCl(OH)_3^-$ is adsorbed into the pores of silica template, and the pore channels limit the growth of Au particles during the calcination process. Following removal of the hard template, the Au particles are embedded or partly enter the Co_3O_4 pore walls. Au particles offer more active sites by entering pores, embedding into pore walls, and drilling through the walls of Co_3O_4 (Figure 3). Seemingly, the well-dispersed gold nanoparticles may be responsible for the enhancement of catalytic activity. It is well-known that active surface oxygen species always exert a great influence on the catalytic activity in low-

temperature oxidation.[47] The activity of the Au/Co_3O_4 catalyst correlates with the surface-active species, i.e., the more a surface-active oxygen species occurs on the catalyst, the higher the catalyst activity. Au nanoparticles dispersed on Co_3O_4 play an important role in promoting the production of active oxygen species on the catalyst surface, which apparently leads to the enhanced oxidation activity of ethylene. It is obvious that the complete oxidation of ethylene to CO_2 occurs on both Co_3O_4 and Au/Co_3O_4 catalysts, which is evidenced by the DRIFT measurements. Consequently, the gold nanoparticles improve the production of surface-active oxygen to increase catalytic activity but do not alter the reaction path of ethylene oxidation.

3. Conclusions

In summary, mesoporous Co_3O_4 and Au/Co_3O_4 catalysts have been successfully synthesized using the nanocasting approach and found to be highly active toward eliminating trace ethylene at 0 °C. Our results show that 30% ethylene conversion on mesoporous Co_3O_4 occurs at 0 °C, but the Co_3O_4 nanosheets prepared by the precipitation method do not have any catalytic activity at 20 °C. Further investigation reveals that the structure control of Co_3O_4 allows improvement of the catalytic activity, i.e., mesoporous Co_3O_4, with reactive planes {110}, are more active than Co_3O_4 nanosheets with {112} planes. Furthermore, the highest activity is found over mesoporous 2.5% Au/Co_3O_4 catalyst (76%) because of the surface-active oxygen species produced easily by the active sites of nanogold on porous Co_3O_4. The obtained mesoporous Co_3O_4 and Au/Co_3O_4 materials are effective low-temperature catalysts, which can break the C−C σ and C−C π bonds at a low reaction temperature, even at 0 °C. These catalytic materials have great potential applications for the efficient elimination of trace ethylene in, for example, warehouse storage. The activation mechanism study in this work helps to understand the improvement of oxide catalyst activity.

4. Experimental Section

Synthesis of KIT-6 Silicas. KIT-6 mesoporous silicas were synthesized using tetraethoxysilane (TEOS) as a silica source and Pluronic P123 ($EO_{20}PO_{70}EO_{20}$) as a structure-directing agent.[48] In a typical synthesis, P123 (0.17 mmol, 1.0 g), *n*-butanol (13.5 mmol, 1.0 g), and HCl (35 mL, 0.6 M) were stirred at 35 °C until a homogeneous mixture formed. TEOS (2.08 g) was then added and stirred for another 24 h at the same temperature, followed by a hydrothermal treatment in an autoclave at 100 °C for 24 h. Following synthesis, the mixture was washed with distilled water until there was no foam in the water used. The sample was then dried and calcined at 550 °C for 3 h to absolutely remove the P123 template. The resulting white powder is 3D cubic KIT-6 mesoporous silica.

Nanocasting Preparation of Mesoporous Au/Co_3O_4 and Co_3O_4. Porous Au/Co_3O_4 materials were prepared using 3D cubic KIT-6 as a hard template. Typically, an aqueous solution of $HAuCl_4 \cdot 3H_2O$ (16.09 mg Au/mL) was adjusted by 1 M NaOH solution to pH 7 and was then dispersed in 21.5 g of 7 wt % solution of $Co(NO_3)_2 \cdot 6H_2O$ in ethanol and stirred at room temperature for 2 h. Subsequently, the KIT-6 was added into the solution containing gold and cobalt precursors. Ethanol was removed by the evaporation at 70 °C for 12 h, and the resulting powder was calcined at 300 °C for 3 h to completely decompose the nitrate species. The impregnation and decomposition steps were repeated once in order to achieve

(47) Chavadej, S.; Saktrakool, K.; Rangsunvigit, P.; Lobban, L. L.; Sreethawong, T. *Chem. Eng. J.* **2007**, *132*, 345–353.
(48) Shi, Y.; Meng, Y.; Chen, D.; Cheng, S.; Chen, P.; Yang, H.; Wan, Y.; Zhao, D. Y. *Adv. Funct. Mater.* **2006**, *16*, 561–567.

perfect nanocasting, but the amount of $HAuCl_4 \cdot 3H_2O$ and $Co(NO_3)_2 \cdot 6H_2O$ used in the repeated step was two-thirds of that used in the first step. The silica template was then removed by etching in 65 mL of 2 M NaOH aqueous solution at 80 °C. The black Au/Co_3O_4 material was recovered by centrifugation and dried at room temperature. The prepared Au/Co_3O_4 material was named as mesoporous $x\%Au/Co_3O_4$ ($x = 1.0, 2.5$), where x is the calculated loading amount of gold, assuming that all the gold and Co_3O_4 were incorporated in the final product. The mesoporous Co_3O_4 samples were prepared by impregnating only $Co(NO_3)_2 \cdot 6H_2O$ in the nanocasting process.

Material Characterization. Wide-angle XRD patterns were measured on X'pert PRO equipment using Cu Kα radiation ($\lambda = 0.15418$ nm) in the 2θ range of 10−70° with a scanning step size of 0.006°. Small-angle XRD was recorded on a X'pert PRO powder diffraction system using Cu Kα radiation in the 2θ range of 0.7−6.0° with a scanning step size of 0.0016°. The textural properties of the samples were measured by N_2 sorption at liquid nitrogen temperature, using a gas adsorption analyzer NOVA 1200. HAADF-STEM and HRTEM micrographs were obtained with a Tecnai G^2 F20 u-TWIN instrument at an accelerating voltage of 200 kV. The specimens were prepared by ultrasonic dispersion in ethanol, evaporating a drop of the resultant suspension onto a carbon support grid. O_2−TPD tests were carried out in Micromeritics Chemisorb 2720 apparatus. Prior to each TPD run, the catalyst was pretreated in the He flow at 300 °C in a quartz reactor. After the reactor temperature was lowered to room temperature, the catalyst adsorbed O_2 for 30 min under O_2 flow of 50 mL·min^{-1}. Then He gas was fed into the reactor at 50 mL·min^{-1} for 30 min to purge any residual oxygen. The catalyst was then heated to 750 °C at a constant heating rate of 10 °C·min^{-1} under He flow of 50 mL·min^{-1}. The desorbed oxygen was monitored by the TCD detector. Infrared spectra of the samples were recorded on a Bruker Tensor27 using the DRIFT technique and scanned from 4000 to 600 cm^{-1} with 256 scans at a resolution of 4 cm^{-1}. Before the DRIFT spectra were recorded, the sample was swept with He gas at 150 °C for 30 min, and then the catalyst bed temperature was lowered to 25 °C. The mixed gas (50 ppm C_2H_4 + 22% O_2 in He), prepared using mass flow controllers with a total gas flow of 60 mL·min^{-1}, was then passed through the sample cell at 25 °C for 20 min.

Activity Measurement of Catalysts for Ethylene Oxidation. Catalytic tests were performed using a fixed bed reactor loading with 0.25 g catalyst (20−40 mesh). The reaction feed consisted of 50 ppm ethylene in synthetic air (O_2: 22%, N_2: balance). The combined gas flow rate was maintained at 60 mL·min^{-1}. The catalyst bed temperature was maintained at 0 °C, and the reactants and products were analyzed by using a gas chromatograph equipped with an FID detector (Porapak-R column). The gas chromatograph was directly connected to a Ni catalyst converter. Conversion was calculated on the basis of ethylene concentration in the effluent.

Supporting Information Available: Low-angle XRD patterns, nitrogen physisorption isotherms, and TEM images of the mesoporous silica KIT-6. This material is available free of charge via the Internet at http://pubs.acs.org.

JA906274T